Supercontinuum generation in benzene-filled hollow-core fibers

Lanh Chu Van,[a] Van Thuy Hoang,[a,b] Van Cao Long,[c] Krzysztof Borzycki,[d] Khoa Dinh Xuan,[a] Vu Tran Quoc,[a] Marek Trippenbach,[b] Ryszard Buczyński,[b,e] and Jacek Pniewski[b,*]

[a]Vinh University, Department of Physics, Vinh, Nghe An Province, Vietnam
[b]University of Warsaw, Faculty of Physics, Warsaw, Poland
[c]University of Zielona Góra, Institute of Physics, Zielona Góra, Poland
[d]National Institute of Telecommunications, Warsaw, Poland
[e]Łukasiewicz Research Network-Institute of Microelectronics and Photonics, Warsaw, Poland

Abstract. Supercontinuum generation (SG) in fused silica photonic crystal fibers (PCFs) having a core infiltrated with liquid benzene is analyzed. Three PCF designs, with dimensions and chromatic dispersion optimized for SG using off-the-shelf femtosecond pulse lasers (1560 nm, 90 ps), are proposed. F1 fiber with lattice constant $\Lambda = 1.5\ \mu$m and linear filling factor $f = 0.45$ has all-normal dispersion and offers SG in the 700- to 2000-nm band at relative power levels within 15 dB when pumped with 3 nJ pulses. F2 fiber ($\Lambda = 1.5\ \mu$m, $f = 0.6$) enables SG in an anomalous dispersion regime, covering 600 to 2600 nm spectral range at relative power levels within 30 dB when pumped with low-energy pulses (1 nJ). The F3 fiber ($\Lambda = 2.5\ \mu$m, $f = 0.6$) also exhibits mostly anomalous dispersion and makes possible SG in a very broad 600 to 3500 nm range at relative power levels within 30 dB when pumped with 2 nJ pulses. © *2021 Society of Photo-Optical Instrumentation Engineers (SPIE)* [DOI: 10.1117/1.OE.60.11.116109]

Keywords: dispersion; benzene; nonlinear optics; photonic crystal fibers; supercontinuum generation.

Paper 20210942 received Sep. 5, 2021; accepted for publication Nov. 9, 2021; published online Nov. 23, 2021.

1 Introduction

Photonic crystal fibers (PCFs) have attracted considerable interest since 2000 as their structure allows for extensive modification of optical properties. In particular, PCFs enable broadband chromatic dispersion engineering by suitable dimensioning and location of holes in the photonic cladding, e.g., to adjust the zero dispersion wavelength (ZDW) to the pump wavelength.[1] It is also possible to obtain all-normal dispersion (ANDi) characteristics for non-solitonic supercontinuum generation (SG).[2]

Hollow-core PCFs open new ways to design fiber-based supercontinuum sources: in addition to the adjustment of the material dispersion component of fiber chromatic dispersion by incorporation of a suitable filler material (as in all-solid glass PCFs[3,4]), the infiltration of the hollow-core with optically non-linear liquid dramatically increases the fiber's non-linearity.

Several liquids have been considered so far. These exhibit simultaneously

- a strong non-linear response compared with fused silica and other glasses used to make fibers, such as lead silicate[5,6] or fluoride glasses[7,8] and
- a low attenuation over a wide range of wavelengths.

In particular, carbon disulfide (CS_2), carbon tetrachloride (CCl_4), nitrobenzene ($C_6H_5NO_2$), toluene ($C_6H_5CH_3$), and chloroform ($CHCl_3$) offer transparency from the visible to the near- or

*Address all correspondence to Jacek Pniewski, j.pniewski@uw.edu.pl

0091-3286/2021/$28.00 © 2021 SPIE

even mid-infrared (up to 12 μm for CCl_4), and high non-linear refractive index up to ca. 2×10^{-18} m^2/W for CS_2.[9] These liquids have been extensively studied as media in non-linear fiber optics because their refractive index is higher than that of fused silica. At first, step-index liquid-core non-linear fibers were developed,[10,11] but such designs allow only limited adjustments of chromatic dispersion. However, in hollow-core fibers with air-glass photonic cladding, it is possible to substantially modify this dispersion[12–14] and hence soliton dynamics in such fibers.[15,16] Hollow core-fiber infiltrated with liquid exhibits not just enhanced non-linearity but also larger mode area compared with solid core PCF, without sacrificing strong non-linear response.[17–21]

As far as we know, use of benzene (C_6H_6) as the core material in PCFs intended for SG in the near-infrared range has not been considered yet. Although the non-linear refractive index of benzene $n_2 = (0.6 \text{ to } 5) \times 10^{-19}$ m^2/W[9,22] is similar to that of toluene or nitrobenzene and lower than that of carbon disulfide CS_2,[9,23–25] the advantage of benzene is low attenuation across a wide spectral range of 0.5 to 14 μm. This is important for SG because it allows free soliton shifts, optical wave breaking, and self-phase modulation (SPM) without attenuation of some parts of spectrum and gradual build-up of supercontinuum along the fiber. One disadvantage of benzene (shared with nitrobenzene, however) is its high freezing point of 5.5°C, which restricts low-temperature applications of filled PCF.

In this paper, we study a potential use of benzene as a core material in highly non-linear PCFs for soliton-based all-normal SG and optimize the fiber design to obtain relatively flat dispersion characteristics, either normal (negative) or anomalous (positive). Finally, we model SG in optimized fibers to determine the limits to spectrum broadening, assuming use of commercially available femtosecond pulsed pump laser operating at 1560 nm, with low-peak power (1 to 3 nJ). Results are compared with performance of liquid core fibers reported previously.

1.1 *Benzene Properties and Liquid Core Fiber Designs*

Benzene is a good candidate for a non-linear liquid filler. Its refractive index is higher than that of fused silica at all wavelengths of interest, so index-guided silica-based PCFs with infiltrated core are feasible. The real part of the linear refractive index n of benzene as a function of wavelength (μm) is calculated using the Cauchy formula as shown in Eq. (1),[26] whereas the Sellmeier formula applies to fused silica glass (SCHOTT Lithosil®), as shown in Eq. (2):

$$n_b^2(\lambda) = A_0 + A_1\lambda^2 + \frac{A_2}{\lambda^2} + \frac{A_3}{\lambda^4} + \frac{A_4}{\lambda^6}, \tag{1}$$

$$n_s^2(\lambda) = B_0 + \frac{B_1\lambda^2}{\lambda^2 - C_1} + \frac{B_2\lambda^2}{\lambda^2 - C_2} + \frac{B_3\lambda^2}{\lambda^2 - C_3}. \tag{2}$$

Parameters $A_0 \ldots A_4$, $B_0 \ldots B_3$, and $C_1 \ldots C_3$ are listed in Table 1. Figure 1 shows the spectral characteristics of the real part of n for liquid benzene at room temperature and fused silica.

We have measured the bulk attenuation of benzene for a sample held in a 10-mm cuvette. The light source was a tungsten halogen lamp, and spectra were acquired with two spectrometers: Thorlabs CCS200 (500 to 1000 nm) and Ocean NIR-QUEST (900 to 2500 nm). The graph of attenuation as the imaginary part of the linear refractive index k is shown in Fig. 2.

The core diameter of a PCF is a trade-off between keeping it:

- small to enable dispersion engineering by design of the photonic cladding and
- large to reasonably match the PCF mode field diameter to telecom single-mode fibers.

Our benzene-infiltrated hollow core PCFs are effective index-guiding PCFs with a reasonably large mode field diameter and chromatic dispersion characteristics matched to pumping with common femtosecond lasers, such as erbium lasers emitting close to 1560 nm.

The central part of the analyzed PCF is shown in Fig. 3. The fiber is made of fused silica, except for the hollow-core being filled with benzene. The photonic cladding consists of eight rings of air holes of a diameter d arranged in a hexagonal lattice with lattice constant Λ. The diameter of the core is defined by the formula $D_c = 2\Lambda - 1.1d$. The linear filling factor of the cladding is defined as $f = d/\Lambda$. In our simulations, we used the lattice constants 1.0, 1.5, 2.0,

Table 1 Chromatic dispersion parameters of liquid benzene and fused silica.

Parameter	Value
Benzene	
A_0	2.170184597
A_1	0.00059399 μm^2
A_2	0.02303464 μm^2
A_3	0.000499485 μm^4
A_4	0.000178796 μm^6
Fused silica	
B_0	1
B_1	0.6694226
B_2	0.4345839
B_3	0.8716947
C_1	4.4801×10^{-3} μm^2
C_2	1.3285×10^{-2} μm^2
C_3	95.341482 μm^2

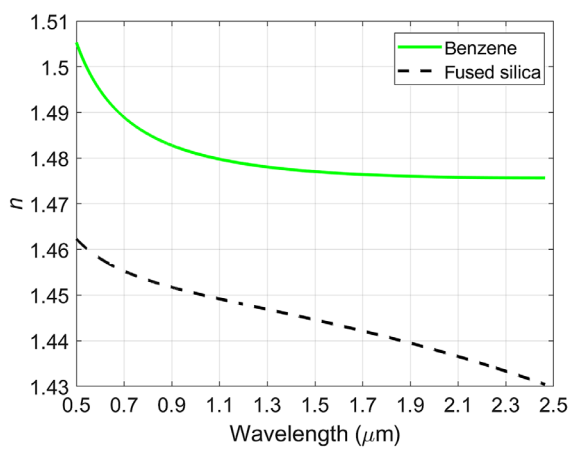

Fig. 1 Real part of the refractive indices n of benzene and fused silica glass.

and 2.5 μm and filling factors 0.3, 0.35, 0.4, 0.45, 0.5, 0.55, 0.6, 0.65, 0.7, 0.75, and 0.8. The smallest core diameter ($D_c = 1.12$ μm) corresponds to $\Lambda = 1.0$ μm and $f = 0.8$, and the largest ($D_c = 4.175$ μm) corresponds to $\Lambda = 2.5$ μm and $f = 0.3$. This range of dimensions takes into account limitations of the stack-and-draw method commonly used for PCF manufacturing.

A commercial eigenmode solver Lumerical MODE was used to calculate modal and dispersion properties of PCFs, with the assumption that benzene introduces negligible losses. This assumption does not influence chromatic dispersion of fibers. Dispersion curves for the fundamental mode are shown in Figs. 4–7. Although chromatic dispersion is mainly influenced by the first (inner) row of air holes surrounding the core, other rows affect mode attenuation, especially for higher order modes[27] and bending conditions.

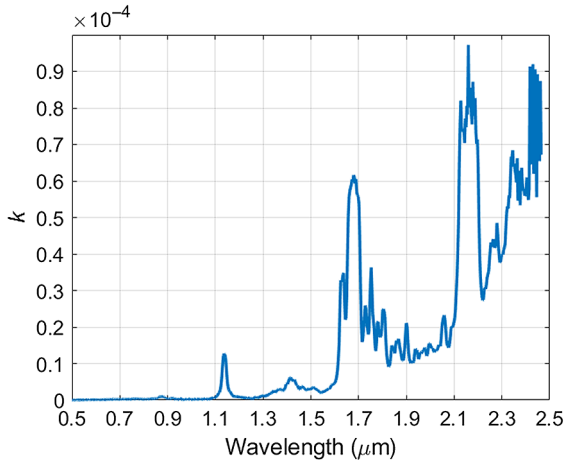

Fig. 2 Imaginary part of the refractive index k of benzene.

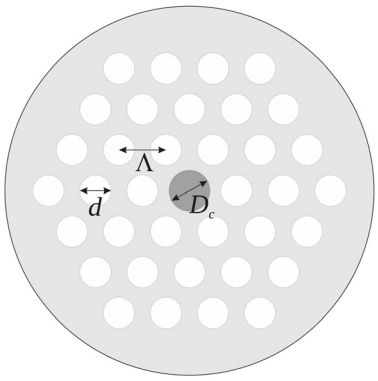

Fig. 3 The structure of PCF with a benzene-infiltrated core (dark gray). Note: only inner three of eight rings of holes (white) in the photonic cladding are shown.

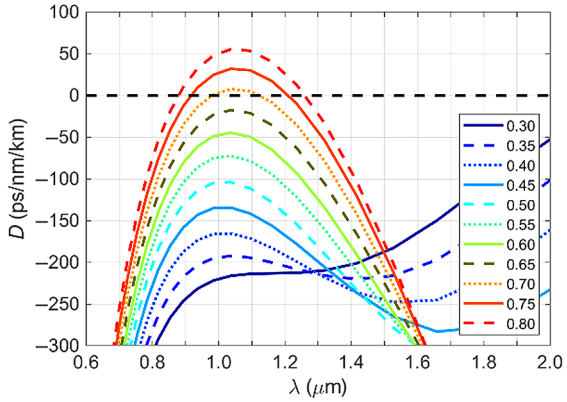

Fig. 4 Chromatic dispersion D of PCF: lattice constant $\Lambda = 1$ μm and filling factor $f = 0.3$ to 0.8.

First, we look for a fiber that could generate a coherent supercontinuum. Such a fiber should have all-normal (negative) chromatic dispersion, with a maximum close to zero in the vicinity of the pump wavelength, a low filling factor supporting single-mode guidance, and a small mode area for high non-linearity. Then we analyze fibers that could keep low anomalous dispersion in wide wavelength ranges, including the intended pump wavelength (1.56 μm). These parameters are attractive for soliton fission (SF)-based SG.

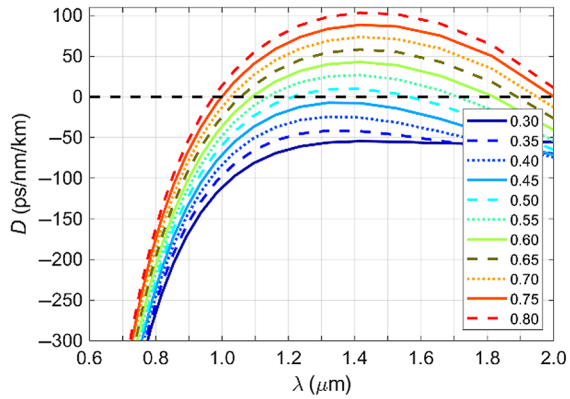

Fig. 5 Chromatic dispersion D of PCF: $\Lambda = 1.5$ μm and $f = 0.3$ to 0.8.

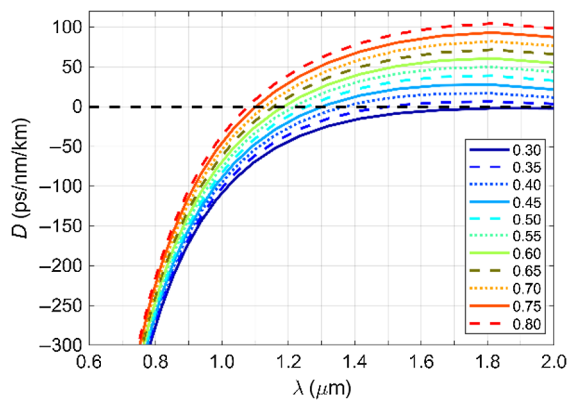

Fig. 6 Chromatic dispersion D of PCF: $\Lambda = 2$ μm and $f = 0.3$ to 0.8.

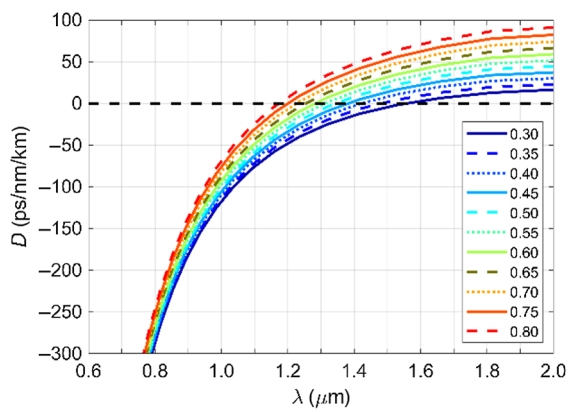

Fig. 7 Chromatic dispersion D for PCF: $\Lambda = 2.5$ μm and $f = 0.3$ to 0.8.

Following the simulations presented above, three PCF designs were selected for further study:

- F1: $\Lambda = 1.5$ μm and $f = 0.45$;
- F2: $\Lambda = 1.5$ μm and $f = 0.6$; and
- F3: $\Lambda = 2.5$ μm and $f = 0.6$.

Dispersion curves of these fibers are shown in Fig. 8.

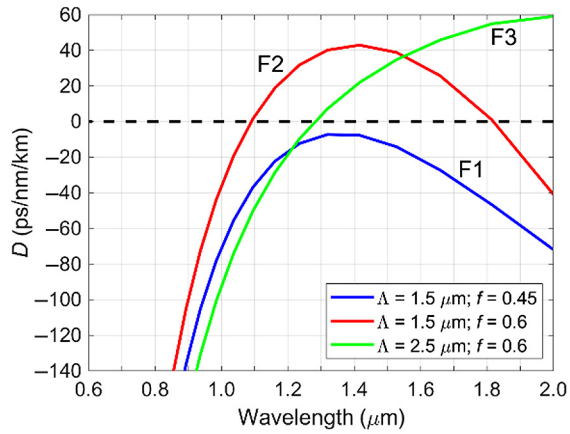

Fig. 8 Dispersion graphs of three fibers selected for SG applications.

They represent the most interesting dispersion options for SG in fibers pumped with fs pulses at 1.56 μm. The F1 fiber has all-normal (negative) chromatic dispersion and a small effective mode area determined by a small lattice constant $\Lambda = 1.5$ μm. A relatively low filling factor $f = 0.45$ ensures single-mode performance. Its numerical aperture (NA), calculated as in Ref. 28, is high at 0.39. Fibers F2 and F3 have anomalous (positive) dispersion over broad ranges of wavelengths, including the intended pump wavelength (1.56 μm). The F2 fiber has high non-linearity due to a small effective mode area and 1.09 to 1.82 μm anomalous dispersion range, whereas F3 exhibits a lower non-linear coefficient due to a large lattice constant $\Lambda = 2.5$ μm and anomalous dispersion at wavelengths longer than its first ZDW of 1.28 μm. NA is 0.43 and 0.28 for the F2 and F3 fibers, respectively.

1.2 *Numerical Modeling of Non-linear Properties of PCFs*

Each of the F1 to F3 fibers has distinct properties and SG applications. The ANDi F1 fiber is expected to enable broadband coherent supercontinuum if pump pulses within the 1200 to 1600 nm range are delivered. The F3 fiber can be used for efficient solitonic SG when pumped with a ytterbium mode-locked laser, whereas F2 with two rather close ZDWs enables a less-explored "arrested soliton" regime of operation, with dynamics that are shaped by SF and dispersive waves (DWs) both at the blue-shifted and red-shifted wings of the pulse spectrum.

For SG modeling, we consider the following parameters of propagation in the fundamental mode: the effective refractive index $n_{\mathrm{eff}}(\lambda)$, effective mode area $A_{\mathrm{eff}}(\lambda)$, chromatic dispersion $D(\lambda)$, and total loss $L_c(\lambda)$. Although the small effective mode area A_{eff} ensures high-power density and efficient SG,[29–31] it unfortunately reduces coupling efficiency of the pump light into the fiber and peak power, especially in a case of large NA mismatch. A careful study is needed to balance the coupling efficiency and non-linear coefficient of the fiber.

SG was numerically analyzed by solving the general non-linear Schrödinger equation. [32] In all cases, pumping with pulses having a 1560 nm central wavelength and 90 fs duration are assumed. Such lasers exist in compact packages and enable rapid development of SG, i.e., the supercontinuum is expected to reach an octave bandwidth in a short ($\leq$5 mm) fiber. This is advantageous in the case of limited peak power coupled to a non-linear fiber and its non-negligible attenuation.

Figure 9(a) shows the evolution of SC spectra in a 1-cm long section of F1 fiber as a function of the input pulse energy varying in the 0.1- to 5-nJ range, corresponding to the peak power of 1.8 to 92.5 kW. For pulse energy below 0.7 nJ, SPM is the main contribution to spectral broadening. In general, the SC spectrum induced by SPM consists of many peaks, with the outermost being the strongest, as shown in Fig. 9(b) for the input pulse energy of 0.5 nJ. At higher input pulse energies, >1 nJ, the SC spectrum is dictated by SPM in the initial stage of propagation and later by optical wave braking (OWB) induced by four-wave mixing (FWM). For the input pulse

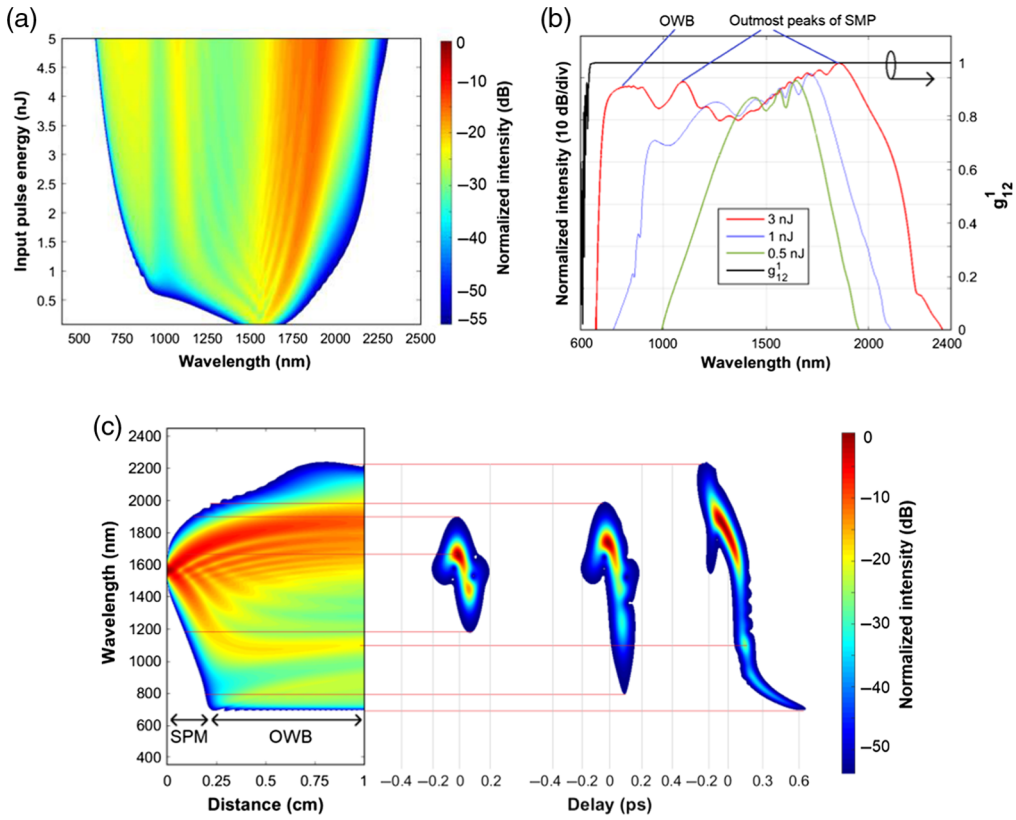

Fig. 9 (a) Evolution of SG along 1 cm of F1 fiber having all-normal chromatic dispersion for various input pulse energies propagation. (b) SC spectra in F1 fiber for different input pulse energies and first-order degree of coherence calculated for 20 individual pulse pairs with random noise. (c) Evolution of pulse in F1 fiber with propagation length for 3 nJ input pulse energy and pulse spectra at three locations along the fiber.

energy of 3 nJ (peak power 55 kW), SC spectrum extends from 700 to 2000 nm with relative power levels within 15 dB and potentially high coherence.[33]

The evolution of SG in the F1 fiber for the 3 nJ input pulse energy is shown in Fig. 9(c). At the beginning of propagation, spectral broadening is produced by SPM, with an S-shaped temporal profile.[2] SC spectrum exhibits clear asymmetry toward the blue side due to non-linear dispersion (self-steepening). Short wavelengths generated by SPM experience strong group-velocity dispersion and travel slower than spectral components of the input pulse tail. When pulse tail and the "slow" components overlap, their interference suddenly generates light at wavelengths around 700 nm at the trailing edge of the pulse via degenerated FWM process, which is attributed to OWB. During further propagation, spectral broadening at the trailing edge of the pulse is limited due to the high slope of dispersion. At the leading edge of the pulse, the wavelength band around 2000 nm is generated by SPM. OWB also occurs and generates a new wavelength band around 2100 nm [Fig. 9(c)]. However, high attenuation and the low non-linear coefficient of the fiber at long wavelengths limit spectral broadening at the leading edge of the pulse.

Pulse spectra at three different locations are shown in Fig. 9(c). The complete SG process includes, from left to right, SPM with the onset of optical wave breaking, the beginning of parametric sideband generation, and the completion of the spectrum by OWB. During further propagation, the light energy is transferred from the central section of the pulse to its edges without generating new wavelength bands. This leads to a flat temporal profile at the trailing end of the pulse.

The F2 fiber has two ZDWs: 1100 nm (ZDW_1) and 1850 nm (ZDW_2), as shown in Fig. 8. The pump wavelength (~1560 nm) falls within the anomalous dispersion regime, and SG in this fiber is generated by soliton dynamics. Figure 10(a) shows the evolution of the spectrum in

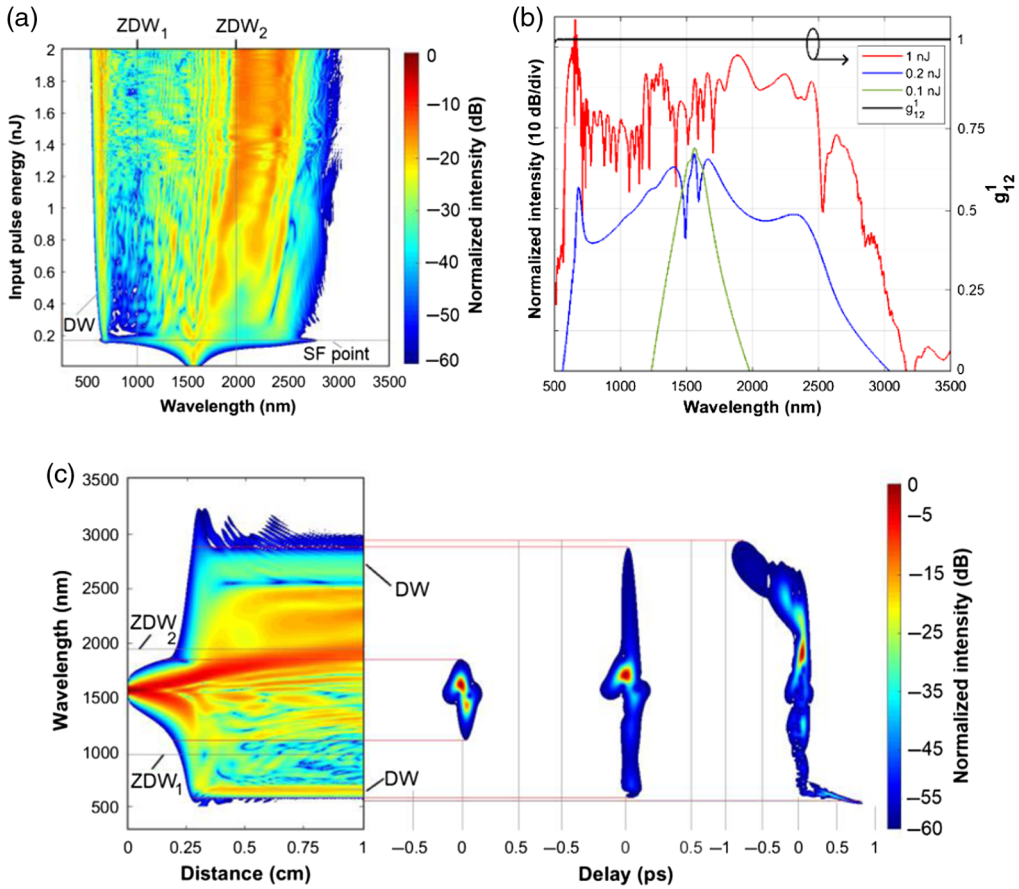

Fig. 10 (a) Evolution of SG in 1-cm long F2 fiber for several input pulse energies. (b) SC spectra generated in F2 fiber for different input pulse energies and first-order degree of coherence calculated with 20 individual pulse pairs with random noise. (c) Evolution of pulse propagating in F2 fiber for 1 nJ input pulse, and pulse spectra at three locations along the fiber.

a 1-cm long fiber for the input pulse energy between 0.01 and 2 nJ, corresponding to peak power in the 0.18- to 37-kW range. SF begins at an input pulse energy of 0.2 nJ and peak power of 2.7 kW. The new wavelength bands in the normal dispersion regime are generated by DW dynamics, but the steep slope of dispersion in this fiber restricts spectral broadening. Consequently, an increase of the input pulse energy changes the structure of the SC spectrum, whereas the spectral bandwidth remains fairly constant [Fig. 10(b)].

The evolution of the pulse propagating in the F2 fiber for the 1 nJ input pulse energy is shown in Fig. 10(c). SPM drives spectral broadening at the beginning of propagation. SF occurs after some 5 mm of propagation, making a dominant contribution to the rapid broadening of the light spectrum. The spectral broadening across ZDW_1 results in the appearance of DW at the trailing edge of the pulse around 600 nm. At the leading edge, the red-shifted DW associated with the negative dispersion slope causes the generation of new wavelengths around 2600 nm. Consequently, as shown in Fig. 10(b), the SC spectrum produced with the 1 nJ input pulse occupies a wide 600- to 2600-nm band with a 30 dB relative power range.

For estimation of coherence properties, the characteristic lengths of the F2 fiber are considered, as given in the following equation:

$$L_D = \frac{t_0^2}{|\beta_2|}, \quad L_{\mathrm{NL}} = \frac{1}{\gamma P_0}, \quad N = \sqrt{\frac{L_D}{L_{\mathrm{NL}}}}, \quad L_{\mathrm{fs}} = \frac{L_D}{N}, \quad L_{\mathrm{MI}} \approx 16 L_{\mathrm{NL}}, \tag{3}$$

where L_D, L_{NL}, L_{fiss}, and L_{MI} are dispersive, non-linear, SF, and MI characteristic length scales, respectively. N is the soliton number. P_0 and t_0 are the peak power and input pulse duration,

Table 2 Non-linear optical parameters of F2 and F3 fibers.

Fiber	P_0 (kW)	β_2 (ps^2/m)	γ (W$^{-1}\cdot$ m^{-1})	N	L_D (cm)	L_{NL} (cm)	L_{fiss} (cm)	L_{MI} (cm)
F2	18.5	−0.0459	0.1064	11	6.4	0.05	0.55	0.81
F3	37	−0.0484	0.0494	10	6	0.054	0.55	0.87

respectively, and β_2 is the group velocity dispersion at the central wavelength of the input pulse. Non-linear parameters of the F2 fiber are shown in Table 2. For the input pulse energy of 1 nJ and peak power of 18.5 kW, we get $L_{\text{fiss}} = 0.55$ cm and $L_{\text{MI}} = 0.81$ cm. This means that SF occurs completely before the noise is amplified by MI. Moreover, noise amplification takes place only in the short-wavelength part of the SC spectrum in the anomalous dispersion regime, ca., 1100 to 1750 nm. Therefore, the SC spectrum generated in the F2 fiber has the potential for high coherence [Fig. 10(b)].

Fiber F3 exhibits a broader wavelength range of anomalous dispersion than F2 with $\text{ZDW}_1 =$ 1280 nm and $\text{ZDW}_2 = 3000$ nm. For input pulse energies above 0.4 nJ, SF and DW become dominant mechanisms of spectral broadening. As in the F2 fiber, the width of the SC spectra is fairly constant irrespective of varying the energy of the input pulse [Figs. 11(a) and 11(b)].

Non-linear parameters of the F3 fiber for the input pulse energy of 2 nJ are listed in Table 2. $L_{\text{fiss}} = 0.55$ cm, in agreement with Fig. 11(c). SF also occurs at this point of propagation, resulting in exceptional spectral broadening: the radiation produced occupies the range from 600 to 3500 nm, extending beyond both ZDWs.

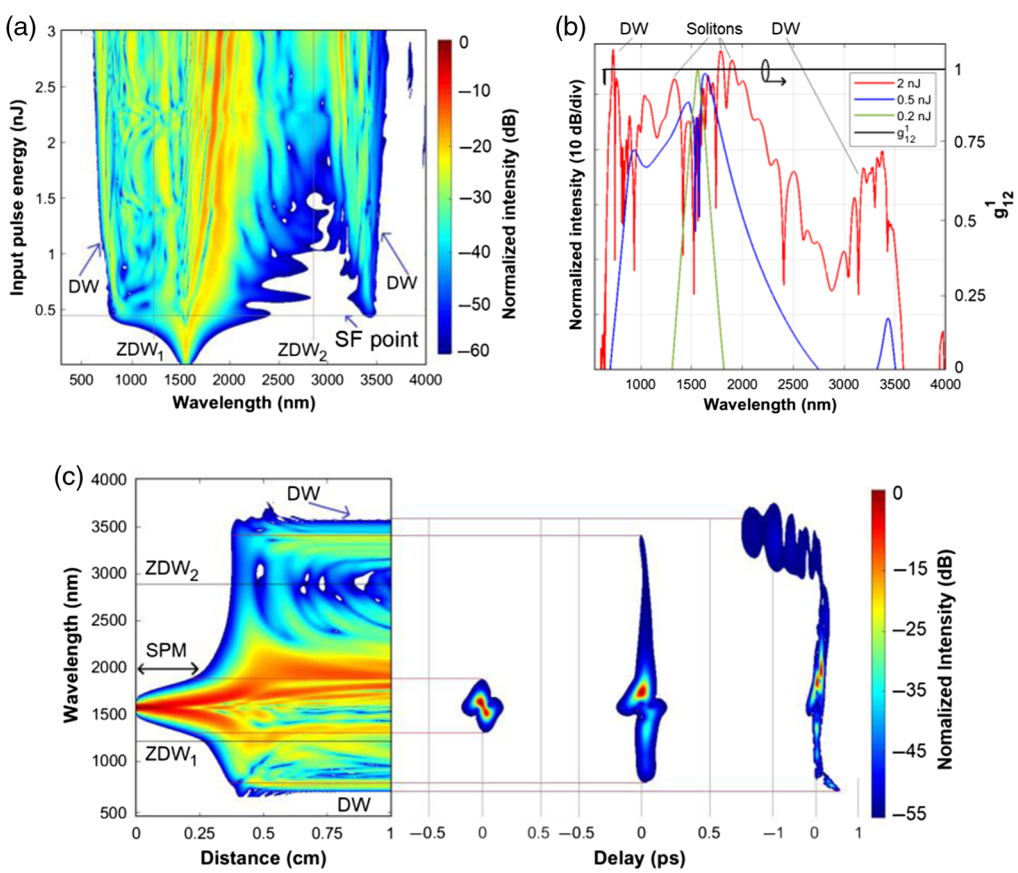

Fig. 11 (a) Evolution of SG along 1 cm of F3 fiber for several input pulse energies. (b) SC spectra produced in F3 fiber for different input pulse energies and first-order degree of coherence calculated with 20 individual pulse pairs with random noise. (c) Evolution of pulse propagating in F3 fiber with length for 3 nJ input pulse and pulse spectra at three locations along the fiber.

For the F2 and F3 fibers, the input soliton number is 10 to 11, which is still reasonable for coherent SG. In all cases, SC bandwidths exceeding an octave were obtained despite limiting pump power to maintain $N \leq 11$. The fiber length is 1 cm, which ensures that $L_{\text{fiss}} < L_{\text{MI}}$ and the influence of fiber attenuation is eliminated.[33,34]

2 Discussion and Conclusions

Benzene is one of the most interesting liquids for non-linear photonics. It has a wide transparency window of 0.5 to 14 μm and a relatively high non-linear refractive index $n_2 = (0.6 \text{ to } 5) \times 10^{-19}$ m^2/W. The toxicity of benzene is moderate with respect to other fillers considered for non-linear fibers with a liquid core, in particular, carbon disulfide (CS_2).

In this paper, we present the optimization of the geometry of fused silica glass-based PCF, in which a hollow core is infiltrated with benzene for use in SG with off-the-shelf femtosecond pulsed lasers. Results show that an optimized hollow-core PCF infiltrated with benzene allows for high flexibility in chromatic dispersion engineering. In particular, low normal or anomalous dispersion can be achieved in a broad range of wavelengths.

We selected three fiber designs with optimized dispersion characteristics and analyzed SG in each when pumped with pulses having a 1560 nm central wavelength and 90 fs duration.

Fiber F1 with the lattice constant $\Lambda = 1.5$ μm and linear filling factor $f = 0.45$ has ANDi characteristics. In this fiber, SG spanning the range of 700 to 2000 nm with relative power levels within 15 dB was achieved for 3 nJ pump pulse energy.

Fiber F2 ($\Lambda = 1.5$ μm, $f = 0.6$) has low anomalous dispersion in the 1.09- to 1.82-μm range, and SG in the range of 600 to 2600 nm with relative power levels within 30 dB occurs when the fiber is pumped with low-energy pulses (1 nJ). This fiber is particularly promising since it combines the broadening efficiency of solitons with the coherence of the ANDi regime.[35]

The third proposed fiber F3 ($\Lambda = 2.5$ μm, $f = 0.6$) exhibits anomalous dispersion between 1280 and 3000 nm. When pumped with 2 nJ pulses, SG in the very broad spectral range of 600 to 3500 nm with relative power levels within 30 dB is predicted.

These SC spectra are broader than in previously analyzed liquid-core PCFs (see Table 3).

Our work shows that hollow core PCFs infiltrated with benzene offer significant flexibility in the design of supercontinuum sources. A supercontinuum broader than two octaves (4:1) can be generated in fibers shorter than 1 cm using low-energy femtosecond pulses $\leq$2 nJ. However, implementation of this approach in all-fiber devices remains challenging since direct coupling of conventional solid fibers to liquid core fibers has not been reported yet. The hybrid approach with optical coupling though reservoir modules was reported,[18] but it requires precise alignment, and miniaturization is necessary to make this technique useful.

Table 3 SC generation reported for PCFs having core infiltrated with non-linear liquids.

Filler	SG spectral range (nm)	Fiber length (cm)	Pump wavelength (nm)	Pump pulse energy (nJ)	Author(s)	Ref.
Toluene	1000 to 1700	1	1550	4	Van et al.	36
Toluene	950 to 1100	10	1030	10	Hoang et al.	18
Nitrobenzene	800 to 2100	5	1560	0.5	Van et al.	37
Carbon disulfide	1460 to 2100	14	1560	7.5	Churin et al.	25
Carbon disulfide	1100 to 2700	14	1950	14	Chemnitz et al.	15
Chloroform	340–1360	1	1060	2.8	Wang et al.	38
Chloroform	600 to 1400	10	1030	1	Lanh et al.	21
Carbon tetrachloride	1000 to 1900	15	1560	3.4	Hoang et al.	39

Acknowledgments

This work was supported by Vietnam National Foundation for Science and Technology Development under Grant No. 103.03-2020.03, Narodowe Centrum Nauki (No. UMO-2016/21/M/ST2/00261), and H2020 ACTPHAST 4.0 (Grant No. 779472). The authors declare no conflicts of interest.

References

1. J. K. Ranka, R. S. Windeler, and A. J. Stentz, "Visible continuum generation in air–silica microstructure optical fibers with anomalous dispersion at 800 nm," *Opt. Lett.* **25**(1), 25–27 (2000).
2. A. M. Heidt et al., "Coherent octave spanning near-infrared and visible supercontinuum generation in all-normal dispersion photonic crystal fibers," *Opt. Express* **19**(4), 3775–3787 (2011).
3. X. Feng et al., "Solid microstructured optical fiber," *Opt. Express* **11**(18), 2225–2230 (2003).
4. M. Klimczak et al., "Coherent supercontinuum generation up to 2.3 μm in all-solid soft-glass photonic crystal fibers with flat all-normal dispersion," *Opt. Express* **22**(15), 18824–18832 (2014).
5. R. Stepien et al., "Soft glasses for photonic crystal fibers and microstructured optical components," *Opt. Eng.* **53**(7), 071815 (2014).
6. J. Cimek et al., "Experimental investigation of the nonlinear refractive index of various soft glasses dedicated for development of nonlinear photonic crystal fibers," *Opt. Mater. Express* **7**(10), 3471–3483 (2017).
7. T. Töpfer et al., "Tailoring the nonlinear refractive index of fluoride-phosphate glasses for laser applications," *Appl. Phys. B* **71**, 203–206 (2000).
8. I. Basaldua et al., "Measurements of the nonlinear refractive index (n2) for indium fluoride (InF3) bulk glass and fiber," in *Front. Opt. Laser Sci.*, Optical Society of America, Paper JTu3A.38 (2018).
9. P. Zhao et al., "Temporal and polarization dependence of the nonlinear optical response of solvents," *Optica* **5**(5), 583–594 (2018).
10. V. F. Zolin and M. A. Samokhina, "Raman spectra in an optical fiber with a liquid core," *Sov. J. Quantum Electron.* **7**, 915 (1977).
11. G. S. He et al., "Stimulated amplification of a broadband optical signal through a benzene-core fiber system pumped by ultra-short laser pulses," *Opt. Commun.* **72**(6), 397–400 (1989).
12. M. Ebnali-Heidari et al., "Dispersion engineering of photonic crystal fibers by means of fluidic infiltration," *J. Mod. Opt.* **59**(16), 1384–1390 (2012).
13. N. Karasawa, "Dispersion properties of liquid-core photonic crystal fibers," *Appl. Opt.* **51**(21), 5259–5265 (2012).
14. J. Pniewski et al., "Dispersion engineering in nonlinear soft glass photonic crystal fibers infiltrated with liquids," *Appl. Opt.* **55**(19), 5033–5040 (2016).
15. M. Chemnitz et al., "Hybrid soliton dynamics in liquid-core fibres," *Nat. Commun.* **8**, 42 (2017).
16. M. Chemnitz et al., "Carbon chloride-core fibers for soliton mediated supercontinuum generation," *Opt. Express* **26**(3), 3221–3235 (2018).
17. H. Zhang et al., "Supercontinuum generation in chloroform-filled photonic crystal fibers," *Optik* **121**(9), 783–787 (2010).
18. V. T. Hoang et al., "All-normal dispersion supercontinuum generation in photonic crystal fibers with large hollow cores infiltrated with toluene," *Opt. Mater. Express* **8**(11), 3568–3582 (2018).
19. H. V. Le et al., "Application of ethanol infiltration for ultra-flattened normal dispersion in fused silica photonic crystal fibers," *Laser Phys.* **28**, 115106 (2018).
20. T. Hoang et al., "Supercontinuum generation in an all-normal dispersion large core photonic crystal fiber infiltrated with carbon tetrachloride," *Opt. Mater. Express* **9**(5), 2264–2278 (2019).

21. C. V. Lanh et al., "Optimization of optical properties of photonic crystal fibers infiltrated with chloroform for supercontinuum generation," *Laser Phys.* **29**, 075107 (2019).
22. E. T. J. Nibbering et al., "Measurement of the nonlinear refractive index of transparent materials by spectral analysis after nonlinear propagation," *Opt. Commun.* **119**(5–6), 479–484 (1995).
23. P. P. Ho and R. R. Alfano, "Optical Kerr effect in liquids," *Phys. Rev. A* **20**, 2170–2187 (1979).
24. S. Couris et al., "An experimental investigation of the nonlinear refractive index (n_2) of carbon disulfide and toluene by spectral shearing interferometry and z-scan techniques," *Chem. Phys. Lett.* **369**(3–4), 318–324 (2003).
25. D. Churin et al., "Mid-IR supercontinuum generation in an integrated liquid-core optical fiber filled with CS_2," *Opt. Mater. Express* **3**(9), 1358–1364 (2013).
26. K. Moutzouris et al., "Refractive, dispersive and thermo-optic properties of twelve organic solvents in the visible and near-infrared," *Appl. Phys. B* **116**, 617–622 (2014).
27. K. Saitoh et al., "Chromatic dispersion control in photonic crystal fibers: application to ultra-flattened dispersion," *Opt. Express* **11**(8), 843–852 (2003).
28. W. J. Wadsworth et al., "Very high numerical aperture fibers," *IEEE Photonics Technol. Lett.* **16**(3), 843–845 (2004).
29. A. Mortensen, "Effective area of photonic crystal fibers," *Opt. Express* **10**(7), 341–348 (2002).
30. N. Naddi, E. Mahammed, and K. L. N. Ksihore, "Dispersion and effective area of air hole containing photonic crystal fibres," *IOSR J. Electron. Commun. Eng.* **12**(3), 09–12 (2017).
31. S. Olyaee and F. Taghipour, "A new design of photonic crystal fiber with ultra-flattened dispersion to simultaneously minimize the dispersion and confinement loss," *J. Phys. Conf. Ser.* **276**, 012080 (2011).
32. J. M. Dudley and J. R. Taylor, *Supercontinuum Generation in Optical Fibers*, Cambridge University Press (2010).
33. J. M. Dudley and S. Coen, "Coherence properties of supercontinuum spectra generated in photonic crystal and tapered optical fibers," *Opt. Lett.* **27**(13), 1180–1182 (2002).
34. A. M. Heidt et al., "Limits of coherent supercontinuum generation in normal dispersion fibers," *J. Opt. Soc. Am. B* **34**(4), 764–775 (2017).
35. R. Johnson et al., "Octave-spanning coherent supercontinuum generation in a silicon nitride waveguide," *Opt. Lett.* **40**(21), 5117 (2015).
36. A. Anuszkiewicz et al., "Photonic crystal fibers with toluene core for nonlinear effects generation," *Proc. SPIE* **10604**, 158–159 (2017).
37. L. C. Van et al., "Supercontinuum generation in photonic crystal fibers infiltrated with nitrobenzene," *Laser Phys.* **30**, 035105 (2020).
38. C.-C. Wang et al., "Numerical simulation of coherent visible-to-near-infrared supercontinuum generation in the $CHCl_3$-filled photonic crystal fiber with 1.06 μm pump pulses," *Opt. Laser Technol.* **88**, 215–221 (2017).
39. V. T. Hoang et al., "Femtosecond supercontinuum generation around 1560 nm in hollow-core photonic crystal fibers filled with carbon tetrachloride," *Appl. Opt.* **59**(12), 3720–3725 (2020).

Lanh Chu Van is an associate professor in the Department of Physics, Vinh University, Vinh, Vietnam. His current research interests include nonlinear optics and photonic crystal fibers and their applications. He has authored and co-authored more than 70 research publications.

Van Thuy Hoang received his PhD in photonics from the University of Warsaw (UoW), Warsaw, Poland, in 2021. His current research interests include nonlinear optics, supercontinuum, generation, and photonic crystal fibers.

Van Cao Long graduated from Warsaw University with an MSc degree in theoretical physics. In 1979, he defended his PhD dissertation in this University. In 1987, he habilitated in the Center of Theoretical Physics, Polish Academy of Sciences in Warsaw. He is an associate professor at the University of Zielona Góra. His research interests concern several topics in quantum and nonlinear optics.

Krzysztof Borzycki received his PhD in communications engineering from the National Institute of Telecommunications (NIT), Warsaw, Poland, in 2006. He has been with NIT since 1982 and currently is an assistant professor in the Metrology Department. His areas of work include FTTx networks, characterization and standardization of fibers, cables and passive components, monitoring and security of fiber networks, effects of extreme temperatures on fibers, and photonic crystal fibers. He is an NIT representative in the Polish Standardization Committee: Cables and Fiber Optics Committees.

Khoa Dinh Xuan graduated in physics from Vinh University, Vinh, Vietnam, in 1981. He completed his PhD in quantum optics in 1996. Since 1997, he has been the head of a research group at Vinh University. He was elected an associate professor in physics in 2003 and a professor in physics in 2015. Currently, he is the vice president of the Vietnam Physics Association. His interests cover quantum and nonlinear optics and atomic and molecular physics.

Vu Tran Quoc obtained his PhD in 2021 from Vinh University. He works at Thu Khoa Nghia Highschool, Châu Đốc, Vietnam. His scientific interests cover optical, electrical, and magnetic properties of nanomaterials, including nonlinear optical effects in photonic crystal fibers. He is an author of more than 13 journal publications and conference papers.

Marek Trippenbach received his PhD from the Polish Academy of Sciences. He worked at the National Institute of Standard and Technology in Gaithersburg and collaborated with William Daniel Phillips, a Nobel Prize Laureate. He is a professor at the Faculty of Physics of the UoW. In 2006, he received the prestigious Wojciech Rubinowicz Prize for his achievements in cold atom physics. He published more than 150 scientific papers, and he is an expert in quantum and nonlinear optics and cold atomic physics.

Ryszard Buczyński received his MSc degree and PhD in physics from Warsaw University of Technology, Warsaw, Poland, in 1994 and 1999, respectively, and his PhD in applied science from Vrije Universiteit Brussels (VUB), Ixelles, Belgium, in 2000. He held postdoc positions at VUB and Heriot-Watt University, the United Kingdom. Currently, he is the group leader at the Institute of Microelectronics and Photonics and Faculty of Physics, UoW, Poland. He leads a research team—Microoptics and Photonic Crystal Fibers Group. His research interests include photonic crystal fibers, supercontinuum generation, microoptics, and optofluidics. He is an author of more than 150 publications.

Jacek Pniewski received his PhD and DSc degree in physics from the UoW, Warsaw, Poland, in 2003, and 2017, respectively. Currently, he works in the Photonics Department of the Faculty of Physics at the UoW. One of his interests is numerical modeling of light propagation in nano- and microoptical devices. He is an author of more than 50 scientific publications.